Microchimica Acta (2022) 189: 285
https://doi.org/10.1007/s00604-022-05365-8

ORIGINAL PAPER

Electrochemical biosensor based on topological insulator Bi_2Se_3 tape electrode for HIV-1 DNA detection

Xiaolu Xiong[1,2] · Peng Zhu[1,2] · Shanshan Li[3] · Yujiu Jiang[1,2] · Yurong Ma[4] · Qingfan Shi[1] · Xu Zhang[1,2] · Xiaoming Shu[3] · Zhiwei Wang[1,2] · Linfeng Sun[1] · Junfeng Han[1,2]

Received: 11 February 2022 / Accepted: 1 June 2022 / Published online: 19 July 2022

Abstract

A large-size Bi_2Se_3 tape electrode (BTE) was prepared by peeling off a $2 \times 1 \times 0.5$ cm high-quality single crystal. The feasibility of using the flexible BTE as an efficient bioplatform to load Au nanoparticles and probe DNA for HIV-1 DNA electrochemical sensing was explored. Differential pulse voltammetry (DPV) and electrochemical impedance spectroscopy (EIS) show that the resultant biosensor has a wide linear range from 0.1 fM to 1 pM, a low detection limit of 50 aM, excellent selectivity, reproducibility and stability, and is superior to the pM DNA detection level of Pt-Au, graphene-AuNPs hybrid biosensors. This outstanding performance is attributed to the intrinsic surface state of Bi_2Se_3 topological insulator in facilitating electron transfer. Therefore, BTE electrochemical biosensor platform has great potential in the application for sensitive detection of DNA biomarkers.

Keywords Electrochemical biosensor · Differential pulse voltammetry · Topological insulator · Bi_2Se_3 tape electrode (BTE) · Au nanoparticles (AuNPs) · HIV-1 DNA

Introduction

Direct Human Immunodeficiency Virus-1 (HIV-1) DNA detection is of great significance for the early diagnosis of AIDS infection preventing the spread of viruses [1–6]. To date, there are a number of ways available for the analysis of HIV-1 DNA. For example, polymerase chain reaction (PCR) [7, 8], surface plasmon resonance [9, 10], and surface-enhanced Raman scattering [11, 12]. Compared to detection strategies mentioned above, the method of electrochemical biosensing has attracted extensive attention due to the merits of higher sensitivity, faster response, lower cost, and simplicity [13–23]. Accordingly, HIV-1 electrochemical biosensors have been fabricated by carbon-based material [24, 25], such as graphene nafion composites [26], $NiCo_2O_4$/CoO@CNTs [27], etc. For the development of high-performance DNA biosensors, it is crucial to explore materials with good conductivity, strong interfacial charge transfer ability, and stable performance.

As a newly emerged exotic material family, topological insulators (Tls) have gained remarkable interest in many fields due to the unique conductive surface states. The electrons on the topological surface state can realize high-speed and low dissipation electron transmission, and are effectively immune to the interference of crystal defects and non-magnetic impurities under the protection of time inversion symmetry [28–30]. These characteristics are the physical basis of electrochemical biosensors with high sensitivity, strong specificity and stability [31, 32]. There were a few research about topological insulator–based electrochemical biosensors. For example, Jiang et al. reported an electrochemical

✉ Zhiwei Wang
zhiweiwang@bit.edu.cn

✉ Linfeng Sun
sunlinfeng@bit.edu.cn

✉ Junfeng Han
pkuhjf@bit.edu.cn

[1] Centre for Quantum Physics, Key Laboratory of Advanced Optoelectronic Quantum Architecture and Measurement (MOE), School of Physics, Beijing Institute of Technology, Beijing 100081, China

[2] Yangtze Delta Region Academy of Beijing Institute of Technology, Jiaxing 314000, China

[3] Department of Rheumatology, China-Japan Friendship Hospital, Beijing 100029, China

[4] School of Chemistry and Chemical Engineering, Beijing Institute of Technology, Beijing 100081, China

biosensor based on exfoliated intrinsic $BiSbTeSe_2$ single crystal with a detection limit of 1.07×10^{-15} M [33]. Compared with other material in the M_2X_3 (M = Bi,Sb, X = Te,Se) family, the carrier mobility of singe crystal $BiSbTeSe_2$ is lower. It is reported that mobility of the best Bi_2Se_3 single crystal can exceed 10^5 cm^2 V^{-1} s^{-1}, which is higher than that of $BiSbTeSe_2$ (4000 cm^2 V^{-1} s^{-1}) [34, 35]. Since the highly mobile surface states can promote interfacial charge transfer and is ideal for electrochemical sensing, Bi_2Se_3 is an excellent candidate for fabricating electrochemical sensor. In addition, Bi_2Se_3 is easier to obtain high quality crystal than quaternary compound, which are conductive to the development of the biosensors. Although the electrochemical biosensors based on Bi_2Se_3 nanoparticles or nanosheets were constructed [36–38], the charge transfer properties of the intrinsic topological surface state are covered by the body state, due to impurities, defects, and grain boundaries in the Bi_2Se_3 nanoparticles or nanosheets. To the best of our knowledge, research of Bi_2Se_3 tape electrode (BTE) stripped from high-mobility Bi_2Se_3 single crystal for the fabrication of ultrasensitive electrochemical biosensors and DNA determination has not been reported.

In this work, we designed a novel electrochemical biosensor based on a Bi_2Se_3 tape electrode (BTE) to detect HIV-1 DNA. As shown in Fig. 1, few-layer Bi_2Se_3 sheets were obtained by peeling off from the crystals. Au nanoparticles were sputtered on BTE to protect the surface state of Bi_2Se_3 and immobilize probe DNA. Due to the protected topological surface state, AuNPs/BTE provides a good pathway of electron transfer towards the target DNA detection. The biosensor here has a series of advantages: (1) Bi_2Se_3 sheets obtained by tape stripping have more uniform quality and high surface area, so as to avoid possible pollution and defects of granular materials prepared by the solvothermal and hydrothermal methods [39–42]. (2) Compared with solid supporting electrodes such as glassy carbon electrodes (GCE) [43], the disposable BTE electrode not only increases the convenience of detection (without polishing before each use), but also improves reproducibility. This work can extend the application of Bi_2Se_3 and Tls in the early diagnosis of diseases.

Experimental

Reagents and apparatus

Bismuth particles and selenium particles with a purity of 5 N were purchased from alfa Co., Ltd. Potassium ferricyanide ($K_3[Fe(CN)_6]$), potassium ferrocyanide ($K_4[Fe(CN)_6]$), potassium chloride (KCl) and phosphate buffer solution (20 × PBS buffer, pH = 7.4) were all obtained from Aladdin Co., Ltd.(Shanghai, China). Ultrapure water (18.2 MΩ cm) was prepared from a Milli-Q system. Tris–EDTA (TE) buffer solution (10 mM Tris–HCl, 1.0 mM EDTA, pH = 8.0) and Normal Human Serum were obtained from Solarbio Biotech Co., Ltd (Beijing, China). All the oligonucleotides related to HIV-1 DNA were synthesized from Sangon Biotech Co., Ltd (Shanghai, China). The detailed sequences of the oligonucleotides [26] were summarized below:

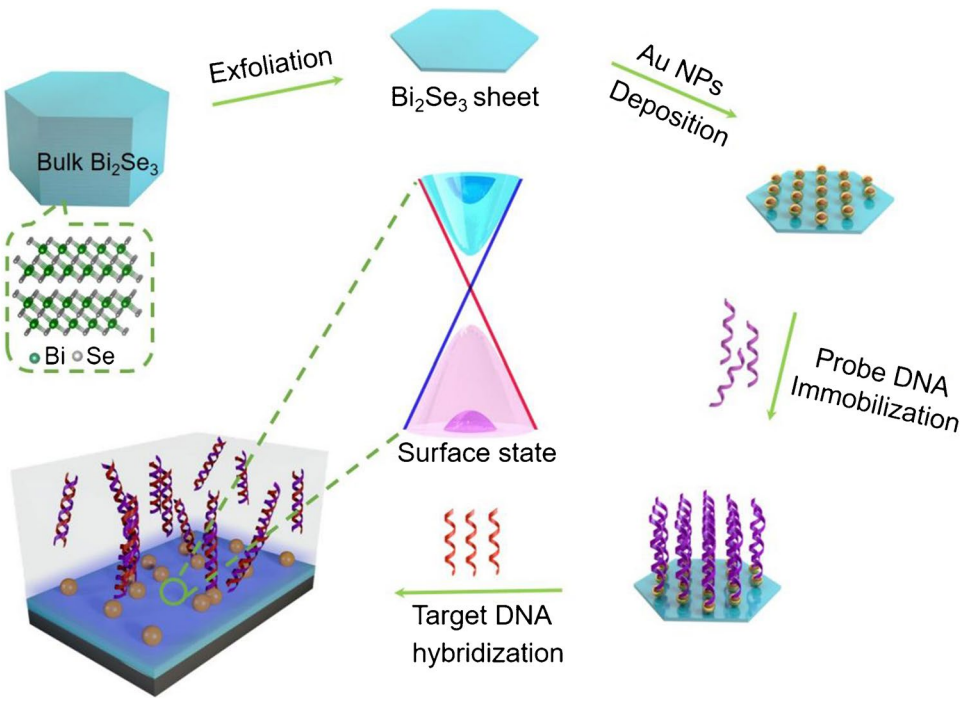

Fig. 1 Schematic illustration of the fabrication of the electrochemical biosensor and the detection of target DNA

Probe DNA (ssDNA): 5′-SH-$(CH_2)_6$-AGT CAG TGT GGA AAA TCT CTA GC-3′.
Target DNA (t-DNA): 5′-GCT AGA GAT TTT CCA CAC TGA CT-3′.
One-base mismatch: 5′-GCT AGA GAT TTT CAA CAC TGA CT-3′.
Three-base mismatch: 5′-GCT CGA GAT TTT CAA CAC GGA CT-3′.

Electrode clamp, Ag/AgCl reference electrode, and pieces of platinum wire auxiliary electrode were bought from GaossUnion Company (Wuhan, China). Au nanoparticles were deposited by a sputtering system (Quorum 150-R, England) at the current of 23 mA for 10 s. The XPS characterizations were performed using a spectrometer (PHI Quatera-II SXM, Japan) with a monochromatic Al K_α X-ray source at a power of 180 W. The morphologies of nanosheets were investigated by TEM (JEM-2011F, Japan). The layers of the nanosheets were explored by Raman (Renishaw InVia, England). Atomic force microscopy (AFM) was used to characterize DNA anchoring on electrode surface (Bruker multimode 8, USA). X-ray diffraction (XRD, Bruker D8 Advance, Germany) was used to detect the crystal phase of Bi_2Se_3.

Synthesis of Bi_2Se_3

The procedure for synthesis of Bi_2Se_3 single crystals has been obtained in detail in the Supplementary information.

Fabrication of the BTE electrochemical biosensor

Bi_2Se_3 sheets were obtained by peeling off from single crystals. Au nanoparticles were sputtered on the Bi_2Se_3 sheets to provide suitable anchoring sites for capture probes. The DNAs were dissolved in TE (pH = 8.0) buffer solution. Afterward, 50 µL of 1×10^{-10} M capture DNA solution was dropped onto the AuNPs/Bi_2Se_3 electrode and incubated for 2 h at room temperature forming Au-SH bonds. Subsequently, the non-specifically absorbed DNA was removed from the electrode surface with filter paper, and the surface was rinsed 3 times with 50 µL ultrapure water (each time) and dried in nitrogen stream. Subsequently, 50 µL HIV-1 DNA solution was added on the surface of ssDNA/AuNPs/Bi_2Se_3 electrode and incubated for another 2 h at 37 ℃ to form dsDNA/AuNPs/Bi_2Se_3 electrode. Finally, the obtained sensor electrode was rinsed carefully according to the above steps and stored in the 4 ℃ refrigerator for further use.

Electrochemical measurements

The prepared biosensor with DNA duplexes on the surface was immersed in an electrochemical cup containing 30 mL of 10 mM PBS (pH 7.40), 5.0 mM $K_4[Fe(CN)_6]$-$K_3[Fe(CN)_6]$, and 0.10 M KCl, with Ag/AgCl as reference electrode and a piece of platinum as counter electrode. Cyclic voltammetry (CV) experiments were carried out at a scan rate of 0.5 V s^{-1} from − 0.2 to 0.6 V. The electrochemical impedance spectroscopy (EIS) experiment was performed with the applied potential of 0.2 V and the frequency of 0.1–10^5 Hz. DPV tests were taken using optimized parameters of pulse amplitude (0.05 V), pulse width (0.05 s), and pulse period (0.5 s).

Sample detection

The application of BTE biosensor was investigated by human serum samples. Firstly, two kinds of human serum samples were prepared by adding HIV-1 DNA (1, 10 pM) to normal human serum samples, respectively. Then, 50 µL prepared serum solution was added onto the ssDNA/AuNPs/Bi_2Se_3 electrode surface and then incubated for 2 h at 37 ℃. Then, the electrode surface was rinsed 3 times with 50 µL ultrapure water and dried in nitrogen. Finally, DPV measurements were carried out and peak current value at potential of 0.25 V is recorded. Each sample was analyzed 5 times.

Results and discussion

Preparation and characterization of Bi_2Se_3 single crystal and AuNP-Bi_2Se_3 electrode

Topological insulators (TIs) are novel exotic materials with insulating bulk but having gapless surface states. Bi_2Se_3 is one of them with a single Dirac cone on its surface states and owns the highest bulk band gap of 0.3 eV among all other TIs materials [44]. It has good biocompatibility, air stability, and very suitable for fabricating ultrasensitive electrochemical biosensors. The synthesized Bi_2Se_3 single crystal is as large as 2 × 1 × 0.5 cm (Fig. 2(a)). The crystal structure was characterized using TEM. As shown in Fig. 2(b), the single crystal has the interplane distance of 0.47 and 0.31 nm, corresponding to the (006) and (009) plane of Bi_2Se_3 crystal, respectively. XRD analysis (Fig. 2(c)) shows that the main diffraction peaks are located at 18.6°, 28.07°, and 47.6° corresponding to the (006), (009), and (0015) crystal faces of hexagonal face-centered Bi_2Se_3 crystal. All the detected peaks (red line) are consistent with those of the Bi_2Se_3 crystal structure (black line, PDF No. 98–016-5226). The exfoliated Bi_2Se_3 sheet is displayed in Fig. 2(d). The high-resolution TEM (HR-TEM) (Fig.2(e)) indicates that the inter-planar spacing lattice distances were 0.24 and 0.31 nm, which agrees well with (111) lattice spacing of Au nanoparticles and (009) plane of Bi_2Se_3, respectively. Besides, the average diameters of Au nanoparticles are in the range of 3–5 nm. The EDS mapping (Fig. 2(f)) confirms that Bi (green) and Se (orange) are homogeneously distributed

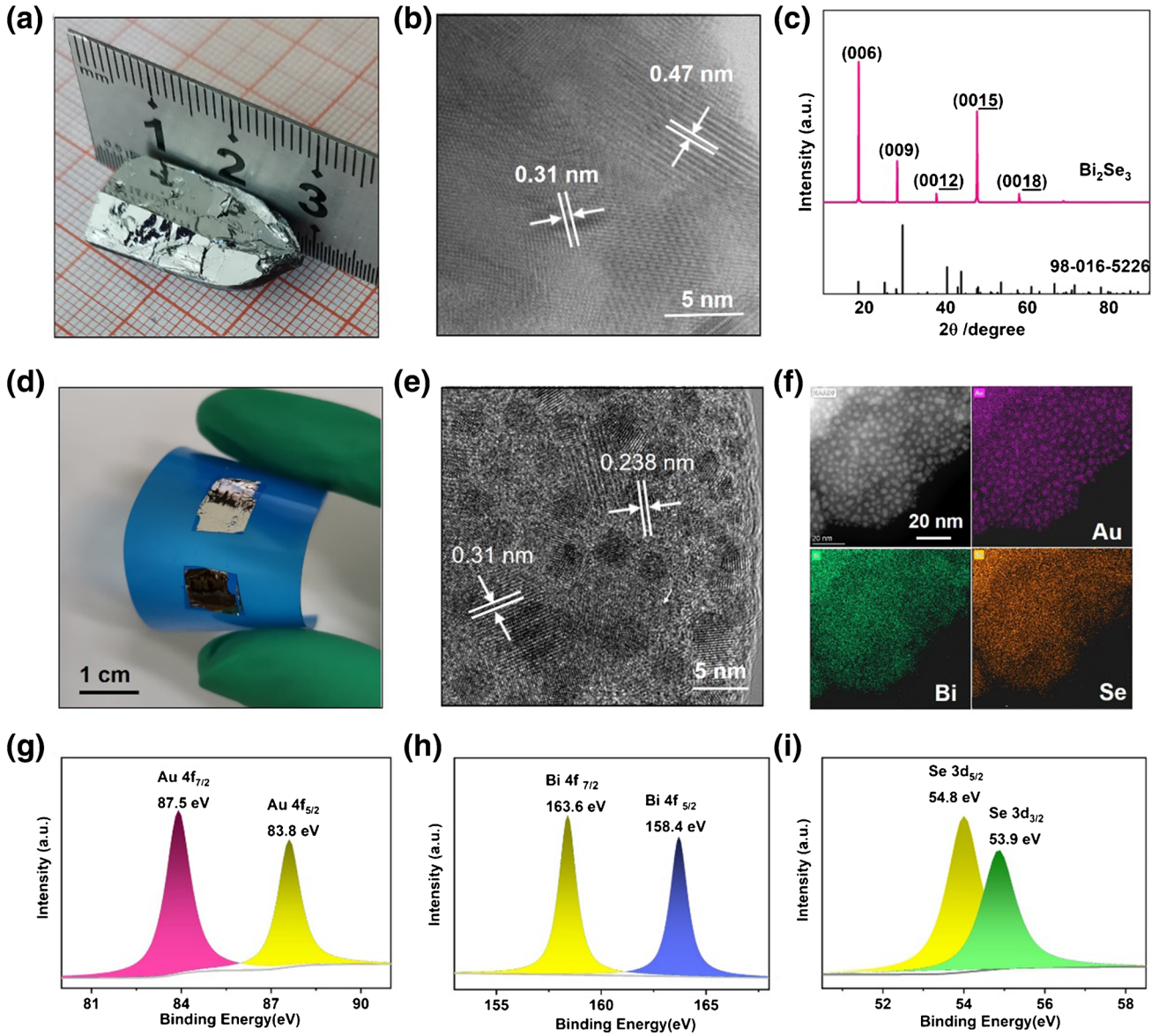

Fig. 2 **a** Photograph of actual Bi_2Se_3 crystal (each small square grid stands for 1 × 1 mm). (**b**) HRTEM image of Bi_2Se_3 crystal. (**c**) XRD of Bi_2Se_3 single crystal. (**d**) Photograph of exfoliated Bi_2Se_3 sheet. (**e**) HRTEM and (**f**) EDS mapping of Bi_2Se_3-AuNPs sheet. The high-resolution XPS spectra of (**g**) Au 4f, (**h**) Bi 4f, and (**i**) Se 3d

over the sheet surface, and Au nanoparticles (purple) are uniformly distributed on the Bi_2Se_3 surface. The corresponding EDS spectrum in Fig. S1 shows the clear peaks of Bi, Se, and Au composition. From the energy spectrum, the atomic ratio of the Bi and Se is 6.4:9.7, which is very close to the Bi_2Se_3 phase. The surface electronic state and composition of Bi_2Se_3-AuNPs sheets were studied by XPS analysis. The survey-scan of XPS spectrum (Fig. S2) demonstrates the coexistence of C, O, Au, Bi, and Se elements for the Bi_2Se_3-AuNPs sheets. Figure 2(g) shows that the core levels at 83.8 eV and 87.5 eV attribute to Au $4f_{7/2}$ and Au $4f_{5/2}$, respectively. As shown in Fig. 2(h), the core levels at 158.4 eV and 163.6 eV correspond to Bi $4f_{7/2}$ and Bi $4f_{5/2}$, respectively, and the peaks located at 54.8 eV and 53.9 eV are related to Se $3d_{5/2}$ and $3d_{3/2}$, respectively (Fig. 2(i)). All these results have good agreement with the literature [36], demonstrating the successful preparation of AuNPs/Bi_2Se_3 electrodes.

Electrochemical analyses of the AuNPs/BTE electrode

Cyclic voltammetry (CV) and EIS techniques were used to investigate the change of electrode behavior during each

assembly step. As displayed in the CV plot, the electrode clamp (Fig. S3a) reveals well-defined redox peaks, the peak-to-peak potential separation is about 100 mV, which confirms the excellent performance of the electrochemical three-electrode system [22]. Compared with the bare electrode clamp, the electrode clamp fixed with AuNPs/BTE (Fig. 3a, purple curve) reveals decreased redox peaks. After the ssDNA was covalently immobilized onto the

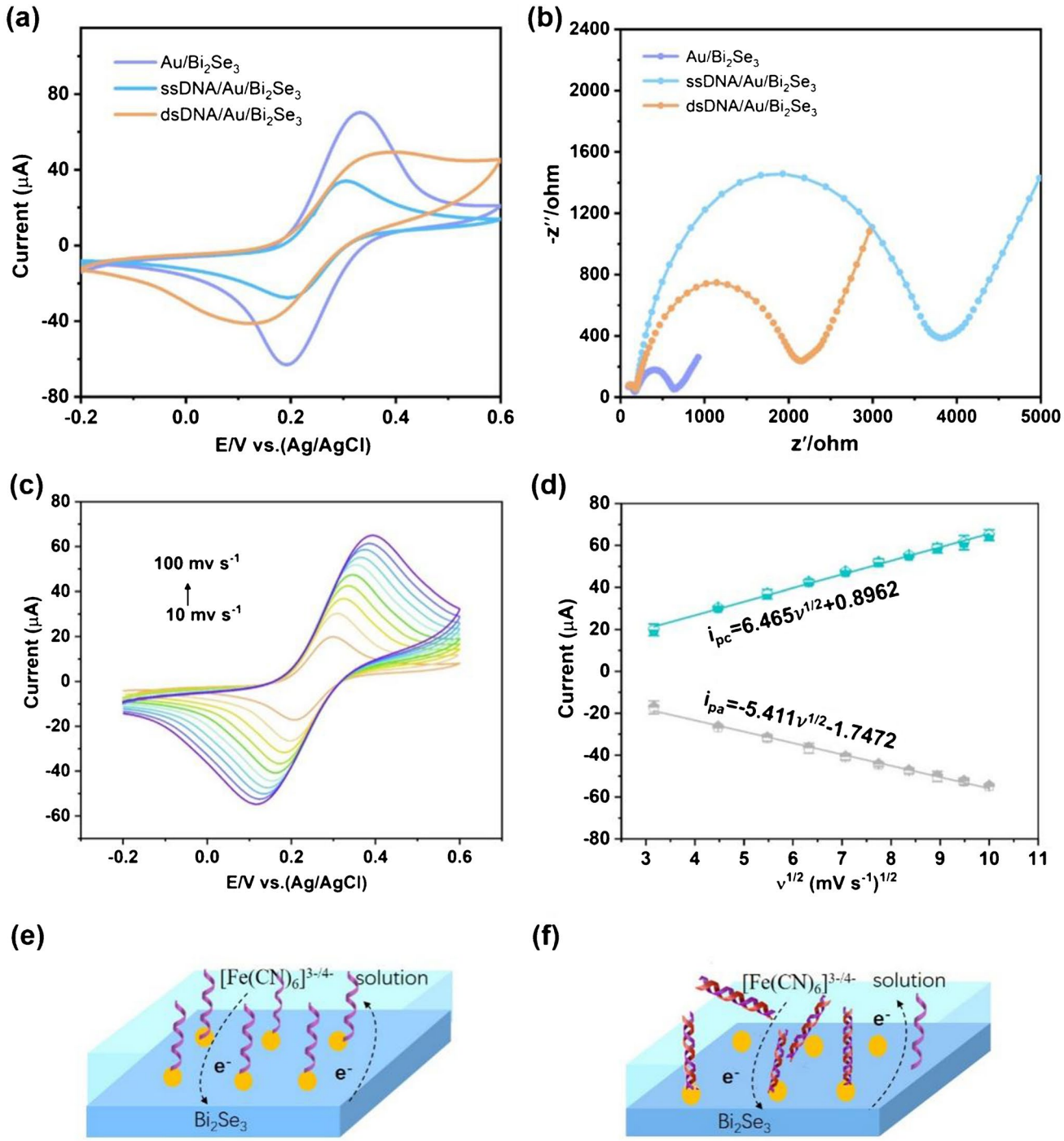

Fig. 3 (**a**) Cyclic voltammograms (CV) curves and (**b**) EIS Nyquist of AuNPs/Bi_2Se_3 (purple color), ssDNA/AuNPs/Bi_2Se_3 (blue color), dsDNA/AuNPs/Bi_2Se_3 (orange color) in 10 mM PBS buffer solution containing 0.1 M KCl and 5 mM $[Fe(CN)_6]^{3-/4-}$. (**c**) CV voltammograms of ssDNA/AuNPs/Bi_2Se_3 electrodes in various scan rates (10, 20, 30, 40, 50, 60, 70, 80, 90, 100 mV s^{-1}). (**d**) Plots of the cathodic and anodic peak currents versus the square root of scan rate ($\nu^{1/2}$). Mechanism of electrode interface change caused by (**e**) ssDNA immobilization and (**f**) dsDNA hybridization

surface of the AuNPs/BTE, the self-redox peaks decrease significantly (Fig. 3a, blue curve). After incubating the ssDNA/AuNPs/BTE with the target HIV-1 DNA, the morphology was recorded by AFM (Fig. S4) and an increase of CV signals was observed clearly (Fig. 3a, orange curve).

EIS is very sensitive to the change of the electron transfer resistance at the electrode/electrolyte interfaces. Figure 3b provided the impedance changes on the electrode during the biosensor construction process. The semicircle features of Nyquist plots can be fitted using a Randles equivalent circuit to extract the electron transfer resistance (R_{et}). The electrode clamp reveals a relatively low resistance (R_{et} = 91.04 Ω, Fig. S3b). When the AuNPs/BTE electrode is bonded on electrode clamp, the resistance obviously increases (R_{et} = 0.63 KΩ, Fig. 3b, purple curve). A sharp increase in semicircle diameter is observed upon the capture ssDNA immobilization on the AuNPs/BTE electrode surface (R_{et} = 3.82 KΩ, Fig. 3b, blue curve). After the hybridization, the R_{et} decreases to 2.15 KΩ (Fig. 3b, orange curve). In all, both CV and EIS analyses claim that the electrochemical biosensor is successfully constructed.

To evaluate the electron transfer kinetics on the surface of AuNPs/BTE, the CV studies on the ssDNA/AuNPs/BTE were further carried out at different scan rates from 10 to 100 mV s^{-1}. Figure 3c indicates that the increase of the scan rate with the steps of 10 mV s^{-1} led to a steady increase in the redox-current peaks. Figure 3d displays the corresponding linear relationships for the reduction current peak (i_p) versus the square root of the scan rate ($\nu^{1/2}$). The calculated linear regression equations for anodes and cathodes are $i_{pc} = 6.465\nu^{1/2} + 0.8972 (R^2 = 0.997)$ and $i_{pa} = -5.411\nu^{1/2} - 1.7472 (R^2 = 0.995)$, respectively. These results indicate that the electrochemical redox process is diffusion-controlled on the surface of AuNPs/BTE electrode [37]. The active surface area of the AuNPs/BTE electrodes was estimated according to the Randles–Sevcik equation [45]:

$$I_P = 2.69 \times 10^5 A D^{1/2} n^{3/2} \nu^{1/2} C \quad (1)$$

Ip is the peak current (μA), A refers to the active surface area (cm^2), D is 6.7×10^{-6}, representing diffusion coefficient (cm^2/s), n is the electron transfer in an electrochemical reaction, ν is scan rate (V/s), and C is the concentration of the $[Fe(CN)_6]^{3-/4-}$ (mol/cm^3). By using the above Eq. (1), the active surface areas were 0.059 cm^2 for AuNPs/BTE electrode.

By studying the relationship between the potential peaks of cathodic and anodic and the logν, the corresponding linear fitting curve is drawn (Fig. S5). The calculated linear regression equations for the cathodic and anodic potentials are $E_{pc} = 0.1332\log\nu + 0.1230 (R^2 = 0.988)$ and $E_{pa} = -0.132\log\nu + 0.3841 (R^2 = 0.991)$, respectively. Using the following equations [27]:

$$\log\frac{k_a}{k_c} = log\frac{\alpha}{1-\alpha} \quad (2)$$

Ka and *Kc* correspond to the slope of $E_{pa} = f(\log\nu)$ and $E_{pc} = f(\log\nu)$, respectively. The charge-transfer coefficient value (α) was calculated as 0.4977 for the AuNPs/BTE electrode.

From the phenomenon observed above, we can explain the main work mechanism of the biosensors. When the ssDNA is covalently immobilized onto the surface of the AuNPs/Bi_2Se_3, the electron transfer between the electrode and $[Fe(CN)_6]^{3-/4-}$ is blocked by the low conductivity of oligonucleotide (Fig. 3e). While incubating the ssDNA/AuNPs/Bi_2Se_3 with the target HIV-1 DNA, dsDNA probably releases from the electrode surface (Fig. 3f), the electron transfer at the electrode interface is enhanced.

Optimization for electrochemical measurements

The detailed evaluation of the effects of capture DNA concentrations, incubation temperature and time was depicted in Fig. S6.

Electrochemical Performance of the BTE/AuNPs biosensor for HIV-1 DNA detection

To investigate the sensitivity of the proposed DNA biosensor, EIS and DPV techniques were performed. In Fig. 4, different concentrations of the target HIV-1 DNA were tested to investigate the performance of the biosensor. The EIS responses of the biosensor to the HIV-1 DNA concentration are displayed in Fig. 4a. As the concentration of the target HIV-1 DNA decreases, the R_{et} increases progressively. By plotting the variation of the R_{et} value between before and after hybridization (namely ΔR_{et}) with the concentration of the HIV-1(Fig. 4c), it is clearly observed that the ΔR_{et} value increases linearly against the logarithmic concentration of HIV-1 DNA in the range from 1.0×10^{-16} to 1.0×10^{-12} M. The linear equation is: ΔR_{et} (Ω) = 310.2 log C (mol/L) + 5822.8 with a correlation coefficient (*R*) of 0.9662.

The DPV technology was used to further validate the sensitivity of the constructed biosensor. In Fig. 4b, the curves show that the DPV peak currents go up correspondingly with the increase of HIV-1 DNA concentrations as well. By plotting the variation of peak current value versus the concentration of HIV-1 DNA, we can conclude that the peak current exhibits good linear relation with the logarithm of HIV-1 DNA concentrations ranging from 1.0×10^{-16} to 1.0×10^{-12} M (Fig. 4d). The regression equation is described as follows: I (μA) = 2.205 log C (mol/L) + 57.31

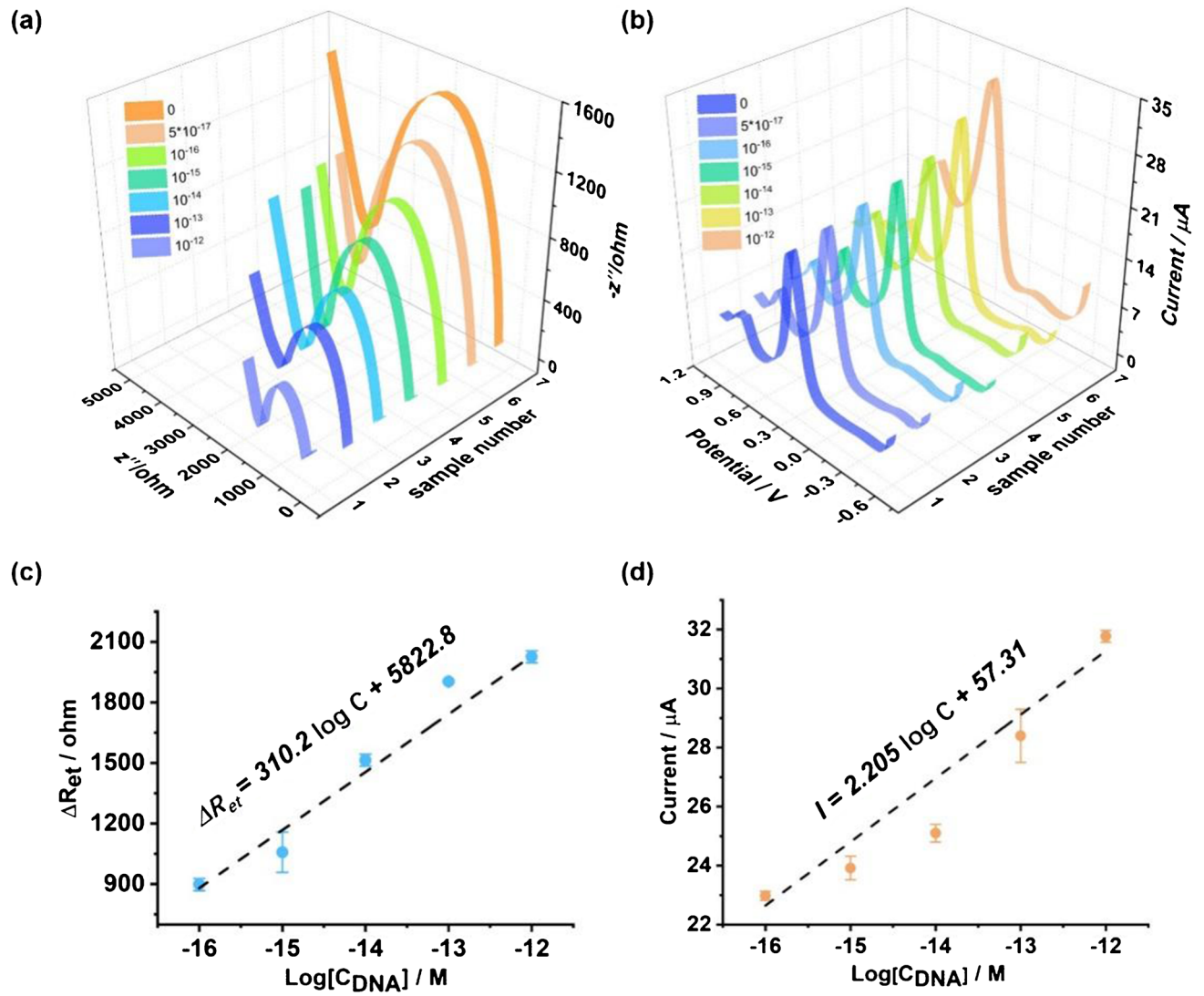

Fig. 4 (**a**) EIS Nyquist plot, and (**b**) DPV response for the detection of different concentrations of HIV-1 DNA (0, 0.05, 0.1, 1, 10, 100, and 1000 fM) using the BTE/AuNPs biosensor. The corresponding linear fit plot of (**c**) ΔR_{et} and (**d**) DPV peak currents obtained as function of the logarithm of HIV-1 DNA concentrations

and the regression coefficient (R) is 0.9292. The detection limit (LOD) was calculated from LOD = 3σ/m, where σ is the standard deviation of DPV blank signal consecutive readings, m is the slope of the calibration plot. LOD was obtained at 0.046 fM (≈ 0.05 fM) based on 3σ/m [37]. In addition, other modified materials and electrochemical techniques for HIV-1 DNA detection were summarized in Table 1. Comparing with the reported electrochemical biosensors, the developed biosensor is quite competitive in detection limit and linear range. This was due to the excellent surface state of topological insulator Bi_2Se_3 facilitating electron transfer.

The selectivity of the constructed biosensors was evaluated with the fully complementary HIV-1 DNA, the one-base mismatched DNA (1 mis DNA) and the three-base mismatched DNA (3 mis DNA), respectively. As displayed in Fig. 5a, the value of ΔR_{et} follows the order of complementary DNA > 1mis DNA > 3 mis DNA > blank, indicating that complete hybridization was not achieved due to the base mismatched, resulting in less double helix formation and reduced value of ΔR_{et}. It can be seen that the constructed biosensor can effectively distinguish target HIV-1 and mismatched DNA. In Fig. 5a, we can find that the peak current of DPV progressively decreases with the increase of the number of mismatched bases. When exactly matched DNA is detected, the peak current of DPV is the highest. When three-base mismatched DNA is detected, the signal of DPV is closer to the bank, indicating that this DNA biosensor has a good distinction between

Table 1 Comparison with reported biosensors based on various electrode materials for the HIV-1 gene detection

Modified electrode	Techniques	Linear range	LODs	Refs
Graphene-Nafion	EIS	0.1 pM–0.1 nM	23 fM	26
EuS nanocrystals	ECL	3 fM–0.3 nM	0.3 fM	46
hpDNA/Au	Amperometry	0.1 pM–10 nM	150 fM	13
$NiCo_2O_4$/CoO/CNTs	EIS	0.1 pM–0.2 nM	16.7 fM	27
GF-CTP-ATP-Au/C-ssDNA	EIS	0.1 pM–10 nM	13 fM	47
NH_2-rGO/beta-CD/GCE	DPV	0.05 pM–1 pM	8.7 fM	25
Au/Bi_2Se_3	**EIS/DPV**	**0.1 fM-1.0 pM**	**0.05 fM**	**This work**

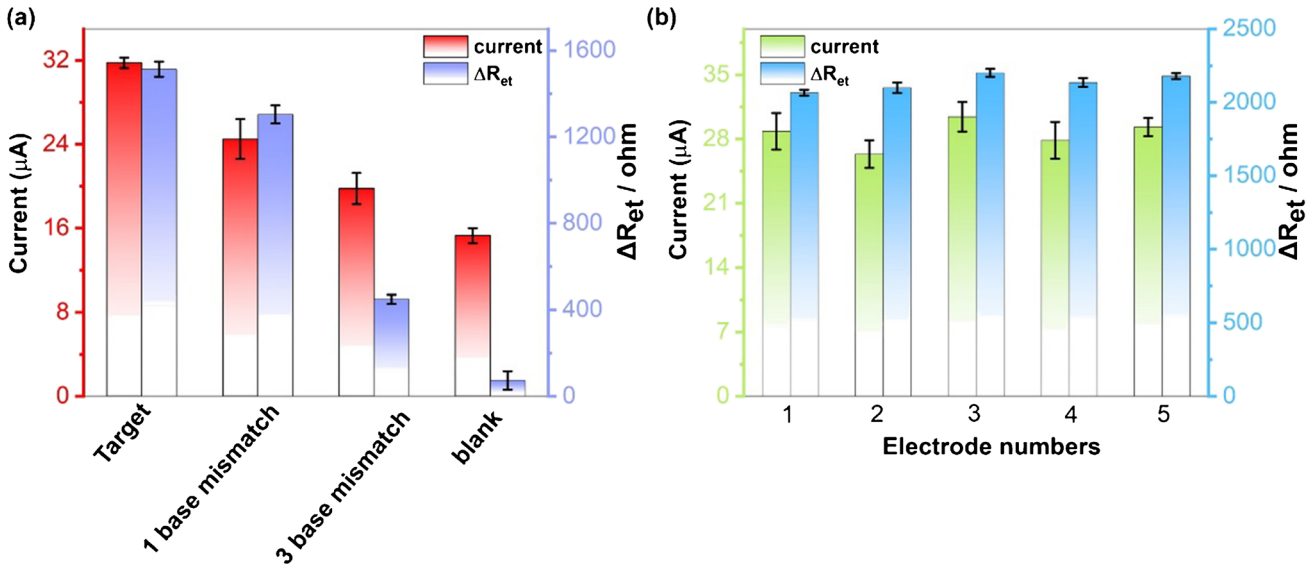

Fig. 5 (**a**) Selectivity of the AuNPs/BTE biosensor: effects of target HIV-1 DNA, one-base mismatched DNA, three-base mismatched DNA and blank on the DPV (red column) and EIS response (purple column), respectively. All the DNA concentration is 1 pM. n = 3. (**b**) The reproducibility of the BTE/AuNPs biosensor for the detection of HIV-1DNA ($n = 5$) measured by DPV (green column) and EIS response (blue column), respectively

mismatched and target DNA. As a result, the BTE biosensor achieved excellent selectivity performance.

The repeatability of the constructed DNA biosensor was measured by detecting 0.1 pM target HIV-1 DNA with five parallel-made probe DNA modified biosensors. The corresponding relative standard deviation values of the EIS and DPV signals were calculated to be 5.25% and 4.57%, separately (Fig. 5b). The results indicate that the biosensor had a desirable repeatability for DNA detection.

The stability and reversibility of the developed biosensor were investigated. It was stored in the refrigerator at 4 ℃ for 9 days. No obvious changes of EIS or DPV signals were observed (Fig. S7), confirming that the DNA biosensor had acceptable stability. The performance of regained biosensor was recorded by DPV voltammograms. The results revealed that the second hybridization efficiency was similar to the first hybridization (Fig. S8), proving that the proposed biosensor has the capability for regeneration and reuse.

To evaluate the practical applications of the proposed BTE biosensor, recovery analysis with real samples was conducted in human serum samples. HIV-1 target DNA (1, 10 pM) was added to healthy human serum samples, respectively. As shown in Table S1, the proposed biosensor exhibited recovery rates ranging from 90.3 to 94.4% in real human serum samples. Since the acceptable recoveries for target analysis were 40–120%, the recoveries of our test samples were satisfactory. These results indicate that the BTE biosensor offers a reliable method for the detection of HIV-1 DNA in biologically relevant samples.

Conclusions

In summary, a novel electrochemical biosensor was developed for HIV DNA detection. Few-layer Bi_2Se_3 sheets were peeled off from Bi_2Se_3 single crystals and decorated with Au

nanoparticles to immobilize capture DNA and selectively recognize target HIV-1 DNA sequence. Owing to unique electrical properties of Bi_2Se_3, the Bi_2Se_3 tape electrode (BTE) facilitates the electron transfer between electrode surface and electrolyte, all of which resulted in a detection limit down to 50 aM and a wide linear range from 0.1 fM to 1 pM towards HIV-1 DNA determination. The proposed biosensor displayed excellent selectivity against mismatched DNA sequences and a sound recovery in human serum. In addition, the reusability and stability of the well-fabricated bio-assay were satisfactory. The proposed BTE electrochemical biosensor provides a promising method to detect HIV-1 DNA at low concentration and extends the sensing applications of topological insulators Bi_2Se_3. Nonetheless, Bi_2Se_3 tape electrode should be further developed to build a portable three-electrode system to facilitate on-site diagnosis and clinic decision-making.

Supplementary Information The online version contains supplementary material available at https://doi.org/10.1007/s00604-022-05365-8.

Acknowledgements We are grateful to the Analysis & Testing Center of Beijing Institute of Technology for the assistance with TEM and XRD analyses.

Funding This work is funded by the National Natural Science Foundation of China (Grant Nos. 11734003, 92065109), the National Key Research and Development Program of China (Grant No. 2020YFA0308800), the Beijing Natural Science Foundation (Grant No. Z210006), and Beijing Institute of Technology Research Fund Program for Young Scholars (Grant Nos. 3180012222011, 3180011182122).

Declarations

Conflict of interest The authors declare no competing interests.

References

1. Ma Y, Shen X, Zeng Q, Wang H, Wang L (2017) A multi-walled carbon nanotubes based molecularly imprinted polymers electrochemical sensor for the sensitive determination of HIV-p24. Talanta 164:121–127
2. Fatin MF, Ruslinda AR, Arshad MK, Tee KK, Ayub RM, Hashim U, Kamarulzaman A, Gopinath CB (2016) HIV-1 Tat biosensor: current development and trends for early detection strategies. Biosens Bioelectron 78:358–366
3. Farzina L, Shamsipurb M, Samandarib L, Shahab S (2020) HIV biosensors for early diagnosis of infection: the intertwine of nanotechnology with sensing strategies. Talanta 206:120201
4. Zhou L, Huang J, Yu B, Liu Y, You T (2015) A novel electrochemiluminescence immunosensor for the analysis of HIV-1 p24 antigen based on P-RGO@Au@Ru-SiO2 composite. ACS Appl Mater Interf 7:24438–24445
5. Li B, Li Z, Situ B, Dai Z, Liu Q, Wang Q, Gu D, Zheng L (2014) Sensitive HIV-1 detection in a homogeneous solution based on an electrochemical molecular beacon coupled with a nafion-graphene composite film modified screen-printed carbon electrode. Biosens Bioelectron 52:330–336
6. Kong MQ, Li ZH, Wu JG, Hu J, Sheng YF, Wu D, Lin Y, Ming L, Wang XZ, Wang SQ (2019) A wearable microfluidic device for rapid detection of HIV-1 DNA using recombinase polymerase amplification. Talanta 205:120155
7. Powell L, Dhummakupt A, Siems L, Singh D, Duff YL, Uprety P, Jennings C, Szewczyk J, Chen Y, Nastouli E, Persaud D (2021) Clinical validation of a quantitative HIV-1 DNA droplet digital PCR assay: applications for detecting occult HIV-1 infection and monitoring cell-associated HIV-1 dynamics across different subtypes in HIV-1 prevention and cure trials. J Clin Virol 139:104822
8. Lee SS, Park JH, Bae YK (2021) Comparison of two digital PCR methods for EGFR DNA and SARS-CoV-2 RNA quantification. Clin Chim Acta 521:9–18
9. Galio L, Briquet S, Cot S, Guilletc J, Vaquero C (1997) Analysis of interactions between huGATA-3 transcription factor and three GATA regulatory elements of HIV-1 long terminal repeat, by surface plasmon resonance. Anal Biochem 253:70–77
10. Zhao YT, Gan SW, Zhang GH, Dai XY (2019) High sensitivity refractive index sensor based on surface plasmon resonance with topological insulator. Results in Physics 14:102477
11. Wabuyele MB, Vo-Dinh T (2005) Detection of human immunodeficiency virus type 1 DNA sequence using plasmonics nanoprobes. Anal Chem 77:7810–7815
12. Yadav S, Senapati S, Desai D, Gahlaut S, Kulkarni S, Singh JP (2021) Portable and sensitive Ag nanorods based SERS platform for rapid HIV-1 detection and tropism determination. Colloids Surf B 198:111477
13. Gao X, Wang X, Li Y, He J, Yu H (2018) Exonuclease I-hydrolysis assisted electrochemical quantitation of surface-immobilized DNA hairpins and improved HIV-1 gene detection. Anal Chem 90:8147–8153
14. Dai Y, Liu CC (2019) Recent advances on electrochemical biosensing strategies toward universal point-of-Care systems. Angew Chem Int Ed 58:12355–12368
15. Li S, Ma L, Zhou M, Li Y, Xia Y, Fan X, Cheng C, Luo H (2020) New opportunities for emerging 2D materials in bioelectronics and biosensors. Curr Opin Biomed Eng 13:32–34
16. Mohammadniaei M, Nguyen HV, Tieu MV, Lee MH (2019) 2D materials in development of electrochemical point-of-care cancer screening devices. Micromachines 10(10):662
17. Chandran GT, Li XW, Ogata A, Penner RM (2017) Electrically transduced sensors based on nanomaterials (2012–2016). Anal Chem 89:249–275
18. Qiao XY, Xia FQ, Tian D, Chen PP, Liu JH, Gu JS, Zhou CL (2019) Ultrasensitive "signal-on" electrochemical aptasensor for assay of acetamiprid residues based on copper-centered metal-organic frameworks. Anal Chim Acta 1050:51–59
19. Blair EO, Corrigan DK (2019) A review of microfabricated electrochemical biosensors for DNA detection. Biosens Bioelectron 134:57–67
20. Wang C, Li YP, Zhao Q (2019) A signal-on electrochemical aptasensor for rapid detection of aflatoxin B1 T based on competition with complementary DNA. Biosens Bioelectron 144:111641
21. Zhang W, Dai ZC, Liu X, Yang JM (2018) High-performance electrochemical sensing of circulating tumor DNA in peripheral blood based on poly-xanthurenic acid functionalized MoS_2 nanosheets. Biosens Bioelectron 105:116–120
22. Liu L, Wei YM, Jiao SL, Zhu SY, Liu XL (2019) A novel label-free strategy for the ultrasensitive miRNA-182 detection based on MoS_2/Ti_3C_2 nanohybrids. Biosens Bioelectron 137:45–51
23. Karaman C, Karaman O, Atar N, Yola ML (2021) Electrochemical immunosensor development based on core-shell high-crystalline graphitic carbon nitride@carbon dots and $Cd_{0.5}Zn_{0.5}S$/d-$Ti_3C_2T_x$ MXene composite for heart-type fatty acid–binding protein detection. Microchimica Acta 188:182

24. Li JF, Lee EC (2017) Functionalized multi-wall carbon nanotubes as an efficient additive for electrochemical DNA sensor. Sens Actuators B 239:652–659
25. Li J, Jin X, Feng M, Huang S, Feng J (2020) Ultrasensitive and highly selective electrochemical biosensor for HIV gene detection based on amino-reduced graphene oxide and β-cyclodextrin modified glassy carbon electrode. Int J Electrochem Sci 15:2727–2738
26. Gong Q, Wang Y, Yang H (2017) A sensitive impedimetric DNA biosensor for the determination of the HIV gene on graphene-Nafion composite film. Biosens Bioelectron 9:565–569
27. Jia ZK, Ma YM, Yang LY, Guo CP, Zhou N, Wang MH, He LH, Zhang ZH (2019) $NiCo_2O_4$ spinel embedded with carbon nanotubes derived from bimetallic NiCo metal-organic framework for the ultrasensitive detection of human immune deficiency virus-1 gene. Biosens Bioelectron 133:55–63
28. Hasan MZ, Kane CL (2010) Colloquium: topological insulators. Rev Mod Phys 82:3045–3067
29. Murakami S, Nagaosa N, Zhang SC (2003) Dissipationless Quantum Spin Current at Room Temperature. Science 301:1348
30. Checkelsky JG, Hor YS, Liu MH, Qu DX, Cava RJ, Ong NP (2009) Quantum interference in macroscopic crystals of nonmetallic Bi_2Se_3. Phys Rev Lett 103:246601
31. Yuan YL, Hu T, Zhong X, Zhu MH, Chai YQ, Yuan R (2020) Highly sensitive photoelectrochemical biosensor based on quantum dots sensitizing Bi_2Te_3 nanosheets and DNA-amplifying strategies. ACS Appl Mater Interf 12:22624–22629
32. Zhou H, Li C, Guo ZM, Wu MH, Li WQ, Xu WP, Liu LF (2018) Bacteria-mediated ultrathin Bi_2Se_3 nanosheets fabrication and their application in photothermal cancer therapy. ACS Sustain Chem Eng 6:4863–4870
33. Jiang YJ, Li SS, Zhu P, Zhao JG, Xiong XL, Wu YT, Zhang X, Li YK, Song TL, Xiao WD, Wang ZW, Han JF (2022) Electrochemical DNA biosensors based on the intrinsic topological insulator $BiSbTeSe_2$ for potential application in HIV determination. ACS Appl Bio Mater 5(3):1084–1091
34. Kim D, Cho S, Butch NP, Syers P, Kirshenbaum K, Adam S, Paglione S, Fuhrer MS (2012) Surface conduction of topological Dirac electrons in bulk insulating Bi_2Se_3. Natural physics 8:459–463
35. Zhang M, Wang X, Zhang S, Gao Y, Yu Z, Zhang X, Gao M, Song F, Du J, Wang X, He L, Xu Y, Zhang R (2016) Unique current-direction-dependent on-off Switching in $BiSbTeSe_2$ topological insulator-based spin valve transistors. IEEE Electr Device L 37(9):1231–1233
36. Xiao LP, Zhu AM, Xu QC, Chen Y, Xu J, Weng J (2017) Colorimetric biosensor for detection of cancer biomarker by Au nanoparticle-decorated Bi_2Se_3 nanosheets. ACS Appl Mater Interf 9:6931–6940
37. Mohammadniaei M, Yoon J, Lee T, Bharate BG, Jo J, Lee D, Choi JW (2018) Electrochemical biosensor composed of silver ion-mediated dsDNA on Au-encapsulated Bi_2Se_3 nanoparticles for the detection of H_2O_2 released from breast cancer cells. Small 14:1703970
38. Zhao FJ, Zhou S, Zhang YJ (2021) Ultrasensitive detection of hydrogen peroxide using Bi_2Te_3 electrochemical sensors. ACS Appl Mater Interf 13:4761–4767
39. Wu SG, Liu G, Li P, Liu H, Xu HH (2012) A high-sensitive and fast-fabricated glucose biosensor based on Prussian blue/topological insulator Bi_2Se_3 hybrid film. Biosens Bioelectron 38:289–294
40. Chen S, Fang YM, Li J, Sun JJ, Chen GN, Yang HH (2013) Study on the electrochemical catalytic properties of the topological insulator Bi_2Se_3. Biosens Bioelectron 46:171–174
41. In C, Sim S, Kim B, Bae H, Jung H, Jang W, Son M, Moon J, Salehi M, Seo SY, Soon A, Ham MH, Lee H, Oh S, Kim D, Jo MH, Choi H (2018) Control over electron-phonon interaction by Dirac plasmon engineering in the Bi_2Se_3 topological insulator. Nano Lett 18:734–739
42. Liu YL, Zhou YY, Zhao ZJ, Zhang QR, Zeng CR, Jia GZ (2020) High-speed shearing prepare Bi_2Se_3 dispersions and effect of size on photothermal conversion. Results in physics 16:103139
43. Wang L, Yu J, Zhang YY, Yang H, Miao LF, Song YH (2017) Simple and large-scale strategy to prepare flexible graphene tape electrode. ACS Appl Mater Interf 9:9089–9095
44. Mazumder K, Shirage PM (2021) A brief review of Bi_2Se_3 based topological insulator: from fundamentals to applications. J Alloys Compd 888:161492
45. Bavandpour R, Karimi-Maleh H, Asif M, Gupta VK, Atar N, Abbasghorbani M (2016) Liquid phase determination of adrenaline uses a voltammetric sensor employing $CuFe_2O_4$ nanoparticles and room temperature ionic liquids. J Mol Liq 213:369–373
46. Babamiri B, Salimi A, Hallaj R (2018) A molecularly imprinted electrochemiluminescence sensor for ultrasensitive HIV-1 gene detection using EuS nanocrystals as luminophore. Biosens Bioelectron 117:332–339
47. Yeter EC, Sahin S, Caglayan MO, Ustundag Z (2021) An electrochemical label-free DNA impedimetric sensor with AuNP-modifed glass fiber/carbonaceous electrode for the detection of HIV-1 DNA. Chem Pap 75:77–87